Article

Chinese Science Bulletin

Geology

December 2013 Vol.58 No.34: 4319–4328
doi: 10.1007/s11434-013-5986-9

Timing of hydrothermal activity associated with the Douzhashan uranium-bearing granite and its significance for uranium mineralization in northeastern Guangxi, China

HU Huan*, WANG RuCheng, CHEN WeiFeng, CHEN PeiRong, LING HongFei & LIU GuoNing

State Key Laboratory for Mineral Deposits Research, School of Earth Sciences and Engineering, Nanjing University, Nanjing 210093, China

Received February 18, 2013; accepted May 20, 2013; published online July 25, 2013

The Miaoershan uranium (U) ore field in northeastern Guangxi is one of the important granite-related U deposits in south China and is closely related to the Douzhashan U-bearing granite. The Douzhashan granite contains primary U-rich accessory minerals, including monazite (UO_2 = 0.98−1.75 wt%) and xenotime (UO_2 = 1.48−6.14 wt%). Primary monazite and xenotime yield chemical ages of 231 ± 28 Ma and 230 ± 38 Ma by electron microprobe analysis and U-Pb isotopic ages of 220±6 Ma and 211±7 Ma by laser ablation-inductively coupled-mass spectrometry respectively. These ages demonstrate that the Douzhashan granite formed during the period of Indosinian magmatic activity. Back scattered electron imaging shows that monazite and xenotime are commonly altered to assemblages of low-U synchisite and apatite, which was associated with loss of U to hydrothermal fluids. U-Th-Pb analyses of secondary apatite yielded a chemical age of 136 ± 17 Ma, which corresponds to the timing of Cretaceous-Tertiary crustal extension in south China. We suggest that the heat and CO_2 required for mineralization was the result of Yanshanian crustal extension, and that this triggered the breakdown of U-rich accessory minerals in the Douzhashan U-bearing granite. Uranium remobilization from the Douzhashan granite provided materials for mineralization within the granite and/or surrounding country rocks. Therefore, a combination of Indosinian compression and Yanshanian extensional overprint produced the hydrothermal U deposits associated with the Douzhashan granite.

monazite, xenotime, apatite, dating, Douzhashan U-bearing granite

Citation: Hu H, Wang R C, Chen W F, et al. Timing of hydrothermal activity associated with the Douzhashan uranium-bearing granite and its significance for uranium mineralization in northeastern Guangxi, China. Chin Sci Bull, 2013, 58: 4319–4328, doi: 10.1007/s11434-013-5986-9

Granite-related uranium (U) deposits are the most important type of U deposit in China. These deposits are found mainly in south China, including those at Zhuguangshan and Guidong in northern Guangdong Province, Taoshan in Jiangxi Province, and Miaoershan in northeastern Guangxi. According to the classification of Cuney [1], granite-related U deposits are a form of hydrothermal vein-type U deposit, and associated granites play a key role in the U mineralization [1–5]. Many recent studies have shown that Indosinian S-type granites are closely related to U metallogenesis [6–10]. Yanshanian tectonism was a post-orogenic geological event related to the Indosinian orogeny. Lithospheric extension at this time produced large-scale magmatism, mineralization agent, heat and favorable space that facilitated U mineralization. As such, the Indosinian granites overprinted by the Yanshanian event are potentially important U source rocks in south China [5,6]. However, a number of questions remain about the nature and origins of the U mineralization, including: (1) What minerals were the U sources in the U-rich granites? (2) How and when was the mineral-bound U released to hydrothermal fluids? (3) What was the nature and timing of the tectono-thermal event related to mineralization? (4) What was the temporal relationship between this tectono-thermal event and crustal extension?

The Miaoershan area is one of five important U ore fields

*Corresponding author (email: huhuan@nju.edu.cn)

in central south China. In this area, the Douzhashan granite is the most prominent Indosinian S-type granite, which is considered to be a potential U source for mineralization. Previous work in the Miaoershan area has mainly involved geochronological, geochemical, and petrogenetic studies of the igneous rocks and related U deposits [11–14]. However, mineralogical studies are relatively scarce and so the present study aims to characterize the occurrences and dating of primary U-rich minerals and their alteration products by electron microprobe (EMP) and multi-collector (MC) laser-ablation (LA)-ICP-MS. Our results on the mineral chemistry, assemblages, and ages of primary monazite and xenotime, and secondary apatite provide new insights into the relationship between the timing of the Yanshanian tectono-thermal event and U mineralization. These results also have implications for the origins of Miaoershan granite-related U mineralization in northeastern Guangxi.

1 Geological setting

The Miaoershan area is located in Ziyuan County in northeastern Guangxi, and is an important site of U, W, and Zn ores in the Nanling region. Tectonically, this region is located at the southern margin of the Jiangnan uplift zone of the Yangtze Plate in southern China.

The Miaoershan plutonic rock complex is the largest igneous unit in the region with an exposed area of 1633 km^2 in the central part of the Miaoershan area. Based on geological investigations, the Miaoershan Complex can be divided into three stages: (1) Caledonian medium- to coarse-grained porphyritic biotite granites; (2) Indosinian medium-grained biotite monzogranites and two-mica monzogranites; and (3) Yanshanian fine-grained biotite or two-mica granites. Uranium mineralization is closely associated with the second-stage Indosinian two-mica monzogranites. To the east, the Xinzi Red Graben Basin is unconformably developed in early Cretaceous strata and contains terrestrial coarse-grained clastic sediments of Cretaceous age. Mafic dikes occur in the central part of the Miaoershan area, including near Guali and Chaping towns. NNE-SSW to NE-SW trending faults were well developed in the area and the Xinzi Fault is the largest fault in the region. The Xinzi Red Graben Basin and Xinzi Fault were favorable sites for the formation of U ore deposits [14,15] (Figure 1).

The Douzhashan granite is one of the Indosinian second-

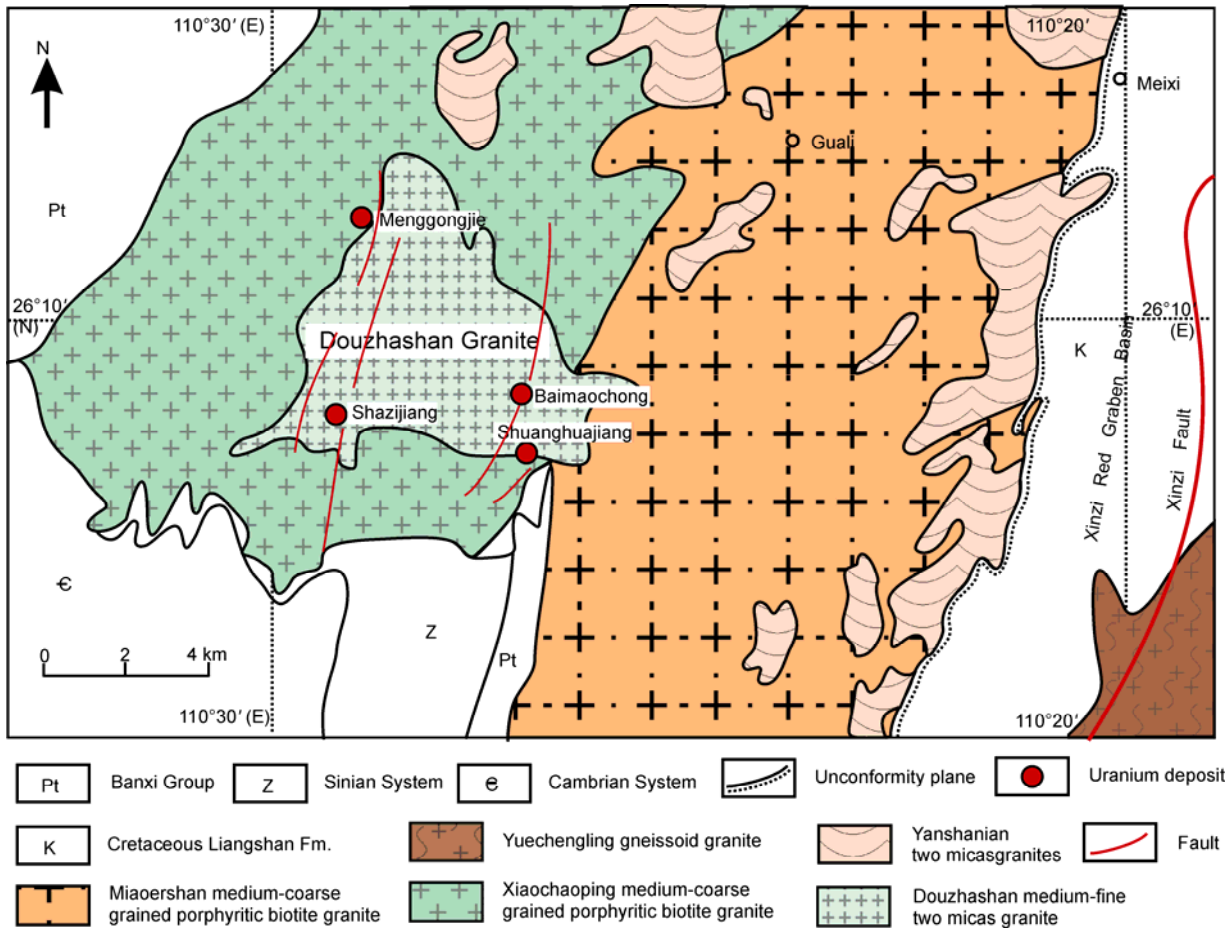

Figure 1 Geological simplified map of the middle of the Miaoershan complex granite (modified from unpublished data of No. 310 Party, Hunuan Nuclear Industry Geological Bureau [17]).

stage granites that intruded the central part of the Miaoershan granitic complex as a stock, and it has an exposed area of 31.7 km^2. The Douzhashan granite mainly comprises medium- to fine-grained, porphyritic, two-mica monzogranite and has a single zircon SHRIMP U-Pb date of 228±11 Ma. Geochemically, the Douzhashan granite is strongly peraluminous and is rich in Si, Al, and alkalis, and poor in Ca, P, Mg, and Ti. The granite has an A/CNK ratio of >1. Geological data indicate that the granite is the late Indosinian crust sourced granite [13].

The U content of the Douzhashan granite is 8.0−23.9 ppm (average = 16.2 ppm), which is an order of magnitude higher than the average U content of upper crust in eastern China (1.6 ppm [16]). Similarly, the Th/U ratio (0.4–3.4, average = 1.9 [13]) of the Douzhashan granite is considerably lower than that of upper crust in eastern China (average=5.8[16]). Several large-scale U deposits (e.g. Shazhijiang, Shuanghuajiang, Baimaochong, and Mengongjie) are all found near the Douzhashan granite (Figure 1). These observations indicate that the Douzhashan granite is a U-rich granite in the Miaoershan granite complex suite, and was potentially the U source for mineralization.

2 Samples and analytical methods

All samples were collected from fresh outcrops of the Douzhashan granite. Polished thin sections were initially examined with an optical microscope and by back-scattered electron (BSE) imaging with an electron microprobe in order to characterize mineral textural relationships and paragenesis. Compositional analyses of accessory and secondary minerals were conducted by electron microprobe analysis. Chemical Th-U-total Pb isochron method (CHIME) and U-Pb isotopic dating of primary monazite and xenotime were performed on the same polished thin sections, but secondary apatite was only dated by the CHIME method because the apatite crystals are too small (several μm) to be analyzed by laser ablation-inductively coupled plasma-mass spectrometry (LA-ICP-MS).

BSE imaging and quantitative mineral chemical analyses were conducted with a JEOL JXA-8100 electron microprobe at the School of Earth Sciences and Engineering, Nanjing University, China. The electron microprobe operating conditions were as follows: accelerating voltage of 15 kV, beam current of 20 nA, and beam diameter of <1 μm; data were corrected using the ZAF method. The standards used were Sri Lanka Zircon for Zr, synthesized ThO_2 for Th, synthesized UO_2 for U, YPO_4 glass for Y, $CePO_4$ glass for Ce and P, and $REEPO_4$ glass for other rare earth elements (REE).

Prior to electron microprobe dating, we optimized the operating conditions to ensure the accuracy of U, Th, and Pb concentration measurements and CHIME ages. The beam diameter for monazite and xenotime was 3 μm, but a smaller beam diameter of 1 μm was used on apatite due to its small size and common presence of thorite inclusions. Given the inverse relationship between detection limits and the square root of counting time [18], we used extended counting times to lower the detection limits (i.e., 100 s on peak and 50 s on background for Th and U; 300 s on peak and 150 s on background for Pb). As some U, Th, and Pb X-ray emission lines partially overlap, particularly the Pb Mα and U Mα lines by the Y Lγ line, we used Th Mα, U Mβ, and Pb Mβ lines to determine the concentrations of these elements [19,20]. The standards used for dating were synthesized UO_2 for U, synthesized ThO_2 for Th, and Pb glass for Pb. The detection limits were 58–60 ppm for U, 33–36 ppm for Th, and 26–28 ppm for Pb. CHIME ages for monazite, xenotime, and apatite were calculated using the program of Kato et al. [21].

Determination of U-Th-Pb isotopic ages on primary monazite and xenotime was performed with an Agilent 7500a LA-ICP-MS coupled to an ArF excimer laser operated at a wavelength of 193 nm, housed at the Institute of Geology and Geophysics, Chinese Academy of Sciences, Beijing, China [22–25]. We used matrix-matched external standards of monazite 4406 and xenotime MG-1. The laser spot size and frequency were 24 μm and 2 Hz, respectively. Each spot analysis comprised ca. 20 s of background data and 65 s of sample data acquisition. Data reduction was carried out with the software package GLITTER 4.0 [26]. $^{206}Pb/^{238}U$ concordia ages and weighted mean ages were calculated with ISOPLOT/EX 3.23 software.

3 Mineral chemistry and paragenesis

The Douzhashan granite comprises K-feldspar, plagioclase, quartz, biotite, and muscovite. The K-feldspar is microcline that has experienced severe argillation. Plagioclase is less abundant than K-feldspar and is mainly albite and oligoclase. Biotite is commonly replaced by chlorite and muscovite, and most biotite is almost completely chloritized. Notably, alteration of accessory minerals is typically located near the chlorite. Figure 2(c) shows how monazite has been largely altered where in contact with chlorite, but is relatively unaltered where in contact with quartz.

Primary accessory minerals are zircon, thorite, apatite, monazite, xenotime, and uraninite. The U-bearing minerals are uraninite, zircon, monazite, and xenotime. The primary mineral U content and hydrothermal alteration are the key factors in assessing the role of these accessory minerals in U mineralization. Given that zircon is unaltered, it cannot have been a U source for mineralization. Electron microprobe analysis shows that monazite and xenotime grains are UO_2 rich and contain 0.98–1.75 wt% and 1.48–6.14 wt% UO_2, respectively, which are generally higher than reported for other similar granites worldwide (monazite UO_2 < 1 wt% and xenotime UO_2 = 1.85–4.71 wt% [27,28]) (Table 1). In

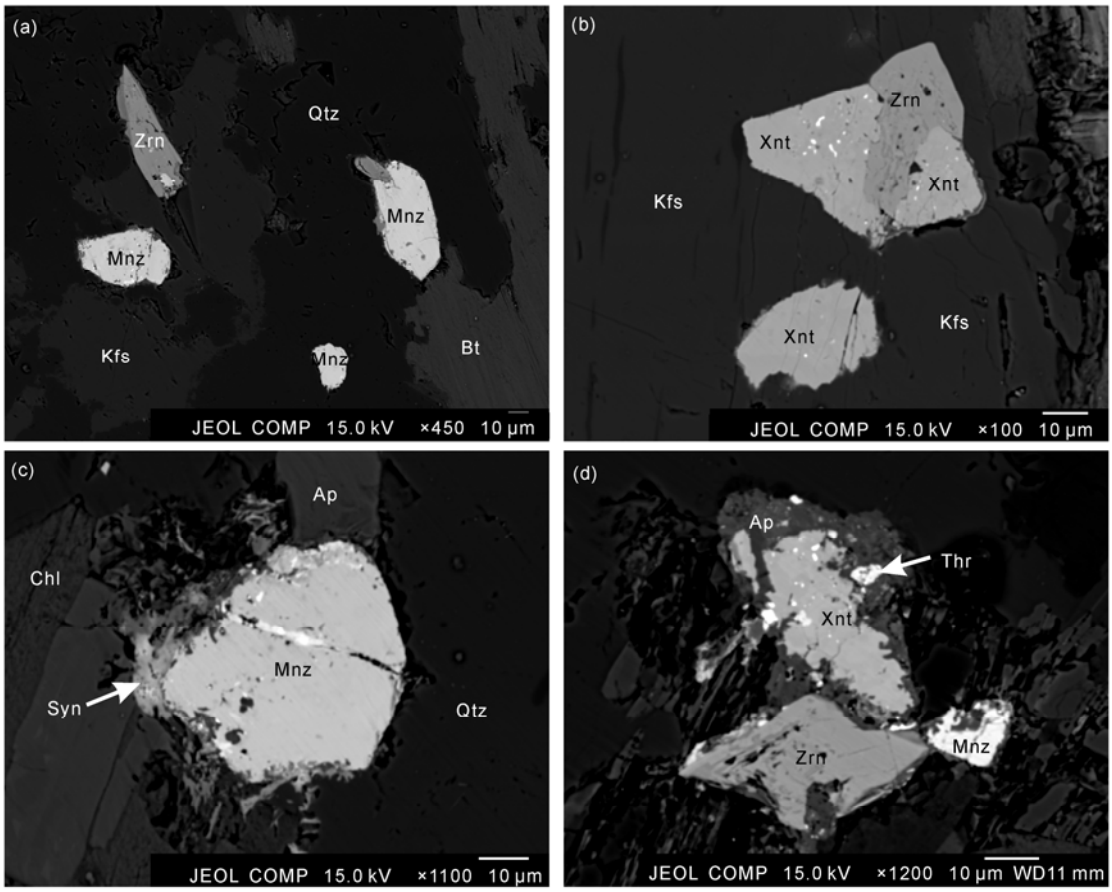

Figure 2 Backscattered electron micrographs of monazite, xenotime andtheir break products from Donzhashan granite. (a) Primary monazite associated zircon with and enclosed in quartz without alteration; (b) primary xenotime and zircon enclosed in K-feldspar; (c) monazite located between quartz and chlorite, monazite alteration is initiated from the margin near the chlorite and partly replaced by synchisite; (d) altered xenotime with a broad rim of secondary apatite; Ap, apatite; Bt, biotite; Chl, chlorite; Kfs, K-feldspar; Mnzmonazite; Qtz, quartz; Sy, synchisite; Thr, thorite; Xnt, xenotime; Zrn, zircon.

addition to their high U content, alteration of monazite and xenotime is also important in U mineralization, so we describe the occurrence and composition of monazite and xenotime and their alteration products in detail later in this paper.

Monazite and xenotime can be subdivided into two types: unaltered and altered. Where these accessory minerals occur as inclusions in feldspar, quartz, and mica, they are unaltered and chemically homogeneous. However, where monazite and xenotime occur among these basic minerals, in particular, nearby chlorite, these accessory minerals are typically altered. Despite this alteration, the electron microprobe results show that the compositions of altered monazite and xenotime cores are still the same as unaltered monazite and xenotime, and have not experienced U loss (Figure 2(a) and (b); Table 1).

The degree of alteration and the breakdown products are different for monazite and xenotime. Monazite alteration has occurred along grain margins or cracks and produced synchisite ($CaCe(CO_3)_2F$) (Figure 2(c)). Xenotime is generally more altered than monazite, and this alteration has typically produced a corona-like appearance with a xenotime core mantled by an apatite rim (Figure 2(d)). UO_2 concentrations in secondary synchisite (detection limit–0.28 wt%) and apatite (0.06–1.99 wt%) are markedly lower than those of primary monazite and xenotime (Table 1). The lower UO_2 concentrations in these secondary products demonstrate that U in the primary minerals was released to hydrothermal fluids during alteration and fed ore-forming fluids that generated late-stage hydrothermal U mineralization.

4 Dating of monazite and xenotime

CHIME and U-Pb isotopic dating were carried out on unaltered monazite and xenotime, and on cores of altered monazite and xenotime (Tables 2 and 3). Nineteen chemical ages for primary monazite range from 193 ± 11 to 244 ± 13 Ma (average = 216 ± 7 Ma). As shown by a plot of PbO versus ThO_2* (Figure 3(a)), the y intercept (i.e. initial Pb) of the isochron is 0.006. This small amount of initial Pb indicates that the CHIME age is reliable and also that there has been no Pb loss during alteration. Using the age calculation program of Kato et al. [21], primary monazite yields a chemical

Table 1 Representative EMPA data (wt%) of monazite, xenotime and secondary poroducts from the Douzhashan granite[a)]

Element	Primary monazite		Margin altered monazite			Primary xenotime		Altered xenotime		
			Unaltered core area	Altered product-synchisite				Unaltered core area	Altered product-apatite	
	1	2	13	3	14	2	4	7	22	24
SiO_2	0.73	0.44	0.74	2.15	4.94	0.43	0.64	0.56	1.08	–
Al_2O_3	–	–	–	0.56	1.93	–	–	–	0.01	0.01
CaO	3.38	1.22	1.70	19.04	16.68	0.17	0.19	0.24	53.40	55.94
FeO	–	–	–	0.68	1.79	n.a.	n.a.	n.a.	n.a.	n.a.
P_2O_5	29.22	30.54	27.33	0.06	0.05	33.16	33.21	33.94	34.91	38.38
UO_2	1.68	1.75	0.98	0.01	0.00	2.06	3.55	2.91	1.62	0.61
ThO_2	15.60	15.94	13.05	4.11	2.45	0.82	1.16	1.21	1.68	0.36
HfO_2	–	–	–	–	–	n.a.	n.a.	n.a.	n.a.	n.a.
PbO	0.07	–	–	–	–	0.41	0.22	0.32	0.08	–
Y_2O_3	2.11	2.51	2.20	3.09	4.64	40.59	41.02	42.06	1.82	0.46
La_2O_3	8.00	8.66	10.81	11.07	8.68	–	–	–	0.04	0.02
Ce_2O_3	19.69	20.51	23.96	20.20	18.62	–	0.02	0.05	0.04	0.04
Pr_2O_3	3.33	3.38	3.45	3.41	2.76	0.03	0.09	–	–	–
Nd_2O_3	9.78	9.54	10.11	10.19	8.46	0.15	0.24	0.35	0.12	–
Sm_2O_3	2.54	2.65	1.83	1.72	1.50	–	–	–	–	–
Gd_2O_3	1.79	1.75	1.24	1.14	1.94	7.15	3.30	3.96	0.71	–
Tb_2O_3	–	–	–	–	–	0.43	0.60	1.12	0.09	0.03
Dy_2O_3	1.73	1.39	1.03	1.70	1.88	5.09	6.25	5.06	0.84	–
Ho_2O_3	–	0.11	0.04	–	–	–	0.21	0.28	0.17	0.19
Er_2O_3	0.23	–	0.06	–	–	4.80	5.01	4.73	–	0.01
Tm_2O_3	0.30	0.18	0.31	0.05	0.08	0.38	0.34	0.39	0.01	–
Yb_2O_3	0.11	–	0.14	–	0.05	3.40	3.69	2.88	0.18	0.16
Lu_2O_3	n.a.	n.a.	n.a.	n.a.	n.a.	0.54	0.75	0.35	0.27	0.05
F	n.a.	n.a.	n.a.	2.47	4.02	–	0.07	–	4.29	4.92
Total	100.28	100.56	99.01	81.64	80.56	99.61	100.54	100.39	101.35	101.18
F=O	0.00	0.00	0.00	1.04	1.69	0.00	0.03	0.00	1.80	2.07
Total	100.28	100.56	99.01	80.61	78.87	99.61	100.51	100.39	99.54	99.12
Si	0.0286	0.0169	0.0303	0.2108	0.4426	0.0148	0.0218	0.0093	0.0972	0.0000
Al	0.0000	0.0000	0.0000	0.0651	0.2032	0.0000	0.0000	0.0000	0.0015	0.0014
Ca	0.1417	0.0507	0.0744	1.9999	1.6000	0.0064	0.0068	0.0042	5.1567	5.1944
Fe	0.0000	0.0000	0.0000	0.0250	0.0604	0.0000	0.0000	0.0000	0.0000	0.0000
P	0.9689	1.0051	0.9439	0.0053	0.0036	0.9706	0.9642	0.2391	2.6635	2.8156
U	0.0146	0.0152	0.0089	0.0002	0.0001	0.0159	0.0271	0.0108	0.0325	0.0118
Th	0.1390	0.1410	0.1211	0.0917	0.0499	0.0065	0.0090	0.0046	0.0344	0.0071
Hf	0.0000	0.0000	0.0000	0.0000	0.0000	0.0000	0.0000	0.0000	0.0000	0.0000
Pb	0.0008	0.0000	0.0000	0.0000	0.0000	0.0038	0.0021	0.0014	0.0018	0.0000
Y	0.0440	0.0518	0.0478	0.1610	0.2212	0.7467	0.7488	0.1863	0.0872	0.0213
La	0.1156	0.1241	0.1627	0.4003	0.2868	0.0000	0.0000	0.0000	0.0013	0.0006
Ce	0.2823	0.2918	0.3579	0.7249	0.6104	0.0000	0.0002	0.0001	0.0012	0.0013
Pr	0.0476	0.0479	0.0513	0.1217	0.0902	0.0004	0.0011	0.0000	0.0000	0.0000
Nd	0.1368	0.1324	0.1473	0.3567	0.2706	0.0018	0.0029	0.0010	0.0039	0.0000
Sm	0.0343	0.0355	0.0257	0.0581	0.0461	0.0000	0.0000	0.0000	0.0000	0.0000
Gd	0.0232	0.0225	0.0168	0.0371	0.0574	0.0819	0.0375	0.0109	0.0213	0.0000
Tb	0.0000	0.0000	0.0000	0.0000	0.0000	0.0049	0.0067	0.0031	0.0025	0.0008
Dy	0.0219	0.0174	0.0135	0.0538	0.0542	0.0567	0.0691	0.0136	0.0243	0.0000
Ho	0.0000	0.0013	0.0005	0.0000	0.0000	0.0000	0.0023	0.0007	0.0048	0.0051
Er	0.0028	0.0000	0.0008	0.0000	0.0000	0.0521	0.0540	0.0124	0.0000	0.0003
Tm	0.0036	0.0022	0.0040	0.0015	0.0023	0.0041	0.0036	0.0010	0.0003	0.0000
Yb	0.0014	0.0000	0.0018	0.0000	0.0013	0.0359	0.0386	0.0073	0.0049	0.0043
Lu	0.0000	0.0000	0.0000	0.0000	0.0000	0.0057	0.0078	0.0009	0.0073	0.0014
F	0.0000	0.0000	0.0000	0.7642	1.1373	0.0000	0.0036	0.0000	0.2259	0.2589

a) –: below detected limit; n.a.: not analyzed; structure chemical formula calculation: anion totals are 4, 6, 4 and 13 for monazite, synchisite, xenotime and apatite respectively.

Table 2 UO_2, ThO_2 and PbO content of monazite and xenotime (wt%) and single-spot Th-U-total Pb ages, ThO_2*, UO_2* calculated from electron-microprobe data

Monazite	UO_2 (%)	ThO_2 (%)	PbO (%)	Apparent age (Ma)	ThO_2^* (%)
1	0.731	11.579	0.139	237±11	13.945
2	0.787	11.872	0.117	193±11	14.411
3	0.669	10.572	0.112	210±12	12.733
4	0.633	10.170	0.108	210±12	12.215
5	0.684	10.663	0.115	213±12	12.873
6	0.679	10.714	0.124	228±12	12.910
7	0.833	11.692	0.128	212±11	14.383
8	0.762	11.654	0.134	226±11	14.118
9	0.76	10.983	0.120	213±11	13.438
10	0.791	10.656	0.118	213±11	13.212
11	0.734	10.533	0.106	196±12	12.901
12	0.678	9.558	0.111	225±13	11.750
13	0.661	10.110	0.112	217±12	12.246
15	0.396	9.798	0.093	200±12	11.076
16	0.684	10.042	0.102	198±13	12.249
17	0.624	10.046	0.124	244±13	12.067
20	0.737	10.138	0.114	217±13	12.520
21	0.718	10.538	0.114	211±12	12.857
22	0.775	11.108	0.135	236±11	13.616
Weight age: 216±7 Ma; isochron age: 231±28 Ma (MSWD = 0.64)					
Xenotime	UO_2 (%)	ThO_2 (%)	PbO(%)	Apparent age (Ma)	UO_2^*(%)
23	1.758	0.591	0.056	213±21	1.941
24	1.843	0.483	0.066	243±20	1.992
26	1.890	0.449	0.066	239±20	2.029
27	1.192	0.322	0.037	212±30	1.292
28	1.853	0.462	0.057	210±20	1.996
29	1.583	0.443	0.051	219±22	1.720
30	1.800	0.432	0.054	206±21	1.934
31	1.984	0.468	0.070	241±19	2.129
32	1.982	0.491	0.065	225±19	2.134
33	1.608	0.471	0.050	210±24	1.754
34	1.092	0.323	0.035	216±35	1.192
35	1.307	0.438	0.043	220±28	1.443
36	1.359	0.486	0.046	225±26	1.509
37	0.994	0.321	0.038	255±36	1.093
38	1.394	0.532	0.049	232±26	1.558
39	1.315	0.504	0.042	211±28	1.471
40	1.700	0.214	0.051	213±22	1.766
Weight age: 223±11 Ma; isochron age: 230±38Ma (MSWD = 0.27)					

isochron age of 231 ± 28 Ma (MSWD = 0.64). Seventeen chemical ages for unaltered xenotime vary from 210 ± 20 Ma to 255 ± 36 Ma (average = 223 ± 11 Ma). Data for xenotime define a linear array on a plot of PbO versus UO_2* and yield an isochron age of 230 ± 38 Ma (MSWD = 0.27) with an intercept of 0.001 (Figure 3(b)).

Monazite and xenotime grains were analyzed *in situ* by LA-ICP-MS to determine U-Th-Pb isotopic ages in the same thin section. Twelve analyses of six monazite grains are all concordant or nearly concordant. The monazite $^{206}Pb/^{238}U$ ages vary between 204 Ma and 233 Ma with a weighted mean age of 220 ± 6 Ma (2σ; MSWD = 2.9) (Figure 4(a)). Eight U-Pb analyses of five xenotime grains yield $^{206}Pb/^{238}U$ ages from 200 Ma to 223 Ma with a weighted mean $^{206}Pb/^{238}U$ age of 211 ± 7 Ma (2σ; MSWD = 2.9) (Figure 4(b)).

The CHIME and the weighted mean U-Pb isotope ages for monazite and xenotime are the same within analytical uncertainties and demonstrate that primary monazite and xenotime formed during the Indosinian.

Table 3 LA-ICP-MS U-Pb analysis data of monazite and xenotime from Douzhashan granite

Spot	U (ppm)	Th (ppm)	Th/U	Isotope ratio								Age	
				$^{206}Pb/^{238}U$	1σ	$^{207}Pb/^{235}U$	1σ	$^{207}Pb/^{206}Pb$	1σ	$^{208}Pb/^{232}Th$	1σ	$^{206}Pb/^{238}U$	1σ
Monazite													
01	3078	115108	37.4	0.03501	0.00091	0.28340	0.00626	0.05871	0.00133	0.01301	0.00026	219.6	5.7
02	4539	135502	29.9	0.03333	0.00082	0.35959	0.00525	0.07825	0.00106	0.01090	0.00022	204.1	5.1
03	4739	134251	28.3	0.03299	0.00081	0.23284	0.00328	0.05118	0.00064	0.01139	0.00023	209.1	5.0
04	5453	130479	23.9	0.03589	0.00088	0.26286	0.00363	0.05311	0.00065	0.01310	0.00026	226.6	5.5
05	5065	126705	25.0	0.03652	0.00089	0.25818	0.00354	0.05127	0.00062	0.01320	0.00026	231.1	5.6
06	5063	122328	24.2	0.03570	0.00089	0.24293	0.00391	0.04935	0.00075	0.01294	0.00026	226.5	5.5
07	4403	112962	25.7	0.03552	0.00088	0.27859	0.00415	0.05688	0.00078	0.01273	0.00025	223.3	5.5
08	5572	142956	25.7	0.03562	0.00090	0.31789	0.00559	0.06471	0.00112	0.01186	0.00024	221.7	5.6
09	4340	109566	25.2	0.03499	0.00089	0.29938	0.00551	0.06206	0.00113	0.01205	0.00024	218.6	5.5
10	4845	133390	27.5	0.03446	0.00085	0.38495	0.00533	0.08100	0.00101	0.01147	0.00023	210.1	5.3
11	4611	125018	27.1	0.03695	0.00092	0.28198	0.00432	0.05535	0.00079	0.01273	0.00025	232.6	5.7
12	6317	123357	19.5	0.03689	0.00135	0.29499	0.01653	0.05798	0.00355	0.01392	0.00032	231.4	8.4
Xenotime													
01	21372	7794	0.36	0.03454	0.00080	0.24528	0.00294	0.05152	0.00053	0.01317	0.00025	218.6	5.0
02	21711	11475	0.53	0.03461	0.00081	0.27183	0.00337	0.05698	0.00062	0.01260	0.00024	217.5	5.0
03	19455	13230	0.68	0.03248	0.00076	0.29244	0.00363	0.06532	0.00071	0.01119	0.00021	202.2	4.7
04	17635	8549	0.48	0.03160	0.00074	0.22504	0.00305	0.05167	0.00063	0.01091	0.00022	200.2	4.6
05	21497	12720	0.59	0.03418	0.00080	0.29242	0.00379	0.06209	0.00072	0.01252	0.00025	213.5	5.0
06	26165	15325	0.59	0.03247	0.00076	0.24559	0.00310	0.05489	0.00060	0.01115	0.00021	204.8	4.8
08	13638	7643	0.56	0.03358	0.00079	0.23427	0.00303	0.05064	0.00058	0.01238	0.00024	212.8	4.9
09	19736	8598	0.44	0.03530	0.00084	0.25034	0.00334	0.05150	0.00061	0.01195	0.00024	223.3	5.2

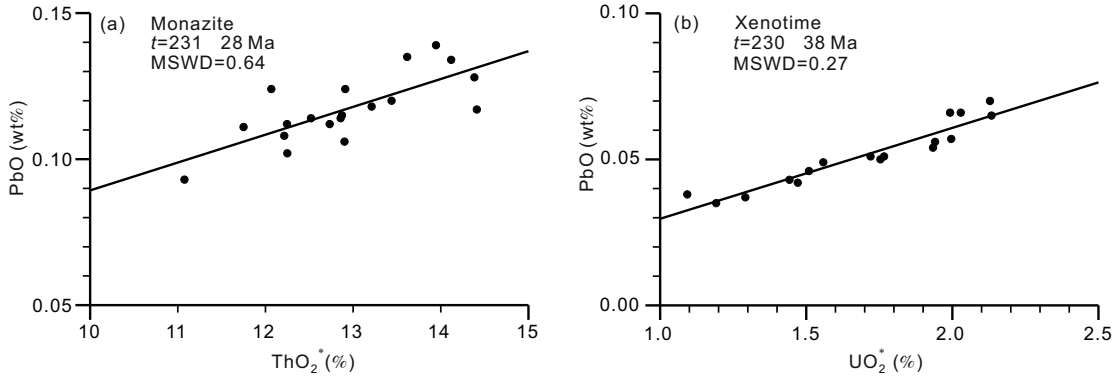

Figure 3 (a) Plot of PbO versus ThO_2^* for monzaite; (b) plot of PbO versus ThO_2^* for xenotime.

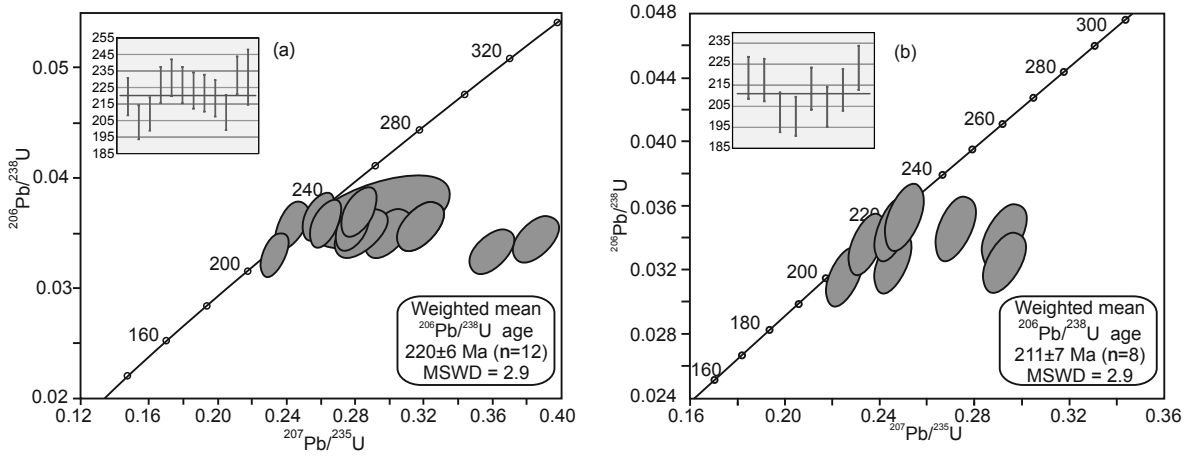

Figure 4 LA-ICP-MS U-Pb dating results of (a) monazites and (b) xenotimes from Douzhashan granite.

5 Dating of secondary apatite

Compared with SHRIMP and LA-ICP-MS dating, CHIME has lower precision but much higher spatial resolution (1–2 μm), and so the latter is suitable for dating very fine-grained material and for investigating intra-crystal heterogeneity and alteration products. To determine the timing of the thermal event that liberated primary U from the monazite and xenotime, it is necessary to date their alteration products. In the Douzhashan granite, synchisite is too small to be dated, but secondary apatite is large enough (up to 10 μm) for CHIME dating.

Secondary apatite is rich in Y (up to 2.47 wt% Y_2O_3; Table 1). These Y contents are obviously higher than that of primary apatite in the Douzhashan granite (average Y = 0.25 wt%), indicating that the secondary apatite inherited the high Y from primary xenotime. Eleven apparent ages for apatite range from 125 ± 17 Ma to 185 ± 14 Ma with a weighted mean age of 140 ± 17 Ma (Table 4). These data form a linear array in a plot of PbO versus ThO_2* (Figure 5), which yields an isochron age of 136 ± 17 Ma (MSWD = 0.52) and an intercept of 0.003. This age is younger than the proposed age of the Douzhashan granite (228 ± 11 Ma [13]); however, it is consistent with the timing of the Yanshanian tectono-thermal event that affected south China (140 Ma [29–31]). This age coincidence suggests that Yanshanian tectonism may have led to the breakdown of primary monazite and xenotime in the Douzhashan granite.

Table 4 UO_2, ThO_2 and PbO content of secondary apatite (wt%), apparent ages, and ThO_2* calculated from electron-microprobe data

Apatite	UO_2 (%)	ThO_2 (%)	PbO (%)	Apparent age (Ma)	ThO_2^* (%)
2	2.185	2.274	0.062	159±16	9.305
3	0.732	0.282	0.019	171±17	2.643
4	2.193	0.784	0.050	152±19	7.838
6	1.471	0.771	0.042	183±24	5.516
9	2.727	0.258	0.047	125±17	9.012
10	2.910	0.071	0.054	137±17	9.420
13	0.868	0.733	0.025	169±24	3.528
15	0.995	0.459	0.020	129±21	3.651
24	0.658	0.424	0.018	170±25	2.543
26	0.435	0.164	0.012	185±14	1.567
45	1.540	0.867	0.037	151±15	5.820

Weight age: 140±17Ma; isochron age: 136±17Ma (MSWD=0.52)

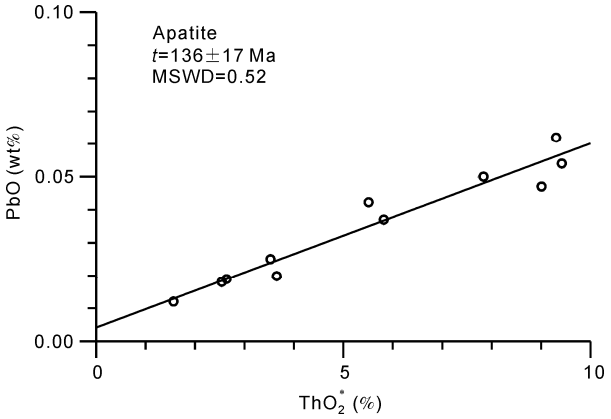

Figure 5 Plot of PbO versus ThO_2^* for secondary apatite.

6 Discussions

6.1 Alteration of monazite and xenotime

Both monazite (Ce) and xenotime (Y) are common REE-rich accessory minerals in granites, pegmatites, migmatites, and low- to high-grade metamorphic rocks [27,28,32–34]. In peraluminous granites, monazite and xenotime are the major host minerals for Y, REE, Th, and U.

During fluid-activated overprinting, monazite and xenotime become unstable as their stability is strongly controlled by temperature, pressure, bulk chemistry, and fluid composition [35,36]. Previous studies have noted that monazite typically breaks down to form apatite-allanite-epidote coronae during low-temperature hydrothermal alteration [27,28,34,37,38]. Compared with monazite, xenotime rarely breaks down into an alteration corona, implying that xenotime has a greater stability than monazite. Xenotime has been documented to breakdown to Y-rich epidote or Y-rich apatite rimmed by Y-rich epidote in granitic rocks of the Western Carpathians, Slovakia [34]. In addition, in the crystalline basement of Athabasca (Canada), Hecht et al. [37] reported that monazite was commonly altered to a Th-silicate phase and that U had been significantly mobilized during alteration and was an important U source for the ore deposit at this site. These previous studies demonstrated that monazite and xenotime alteration controlled the redistribution of P, Y, REE, Th, and U during mineral-fluid interactions.

During the magmatic evolution stage of the Douzhashan granite, monazite and xenotime, while included in rock-forming minerals, are stable. However, during alteration of the granites, both xenotime and monazite became unstable. Petrographic observations suggest that the breakdown of monazite to synchisite and the breakdown of xenotime to apatite were accompanied by the chloritization of biotite. The presence of synchisite and apatite indicates that the alteration was possibly triggered by F-CO_2-rich and Ca-bearing fluids. Previous studies have recognized that Ca is released during the transformation of biotite to chlorite [39,40]. In the case of south China, isotopic, fluid inclusion, and other geological data suggest that such CO_2-enriched fluids were probably directly or indirectly derived from the mantle and not from silicic magmas [41–43]. CO_2 from the mantle is a highly effective mineralizing agent, and >95% of the U in the early stage fluids was transported as $UO_2(CO_3)_2^{2-}$ and $UO_2(CO_3)_3^{4-}$ complexes during hydro-

thermal migration of U [30,42,44–46]. By modifying the reactions presented in Veblen and Ferry [47] and Lanzirotti et al. [40], the breakdown of monazite and xenotime can be expressed as follows:

$$(U,Ce)PO_4\ (\text{monazite}) + K(Mg,Fe)_3(Si_3AlO_{10})(OH)_2\ (\text{biotite}) + Ca^{2+} + F^- + 2CO_3^{2-} \rightarrow (Mg,Fe)_6(Si_3AlO_{10})(OH)_8\ (\text{chlorite}) + CaCe(CO_3)_2F\ (\text{synchisite}) + K^+ + U^{4+} + P^{5+}$$

$$(U,Y)PO_4\ (\text{xenotime}) + K(Mg,Fe)_3(Si_3AlO_{10})(OH)_2\ (\text{biotite}) + Ca^{2+} + F^- \rightarrow (Mg,Fe)_6(Si_3AlO_{10})(OH)_8\ (\text{chlorite}) + (Y,Ca)_2(PO_4)_3(F,OH)(\text{Y–apatite}) + K^+ + U^{4+}$$

As such, U in accessory minerals was released during alteration as $UO_2(CO_3)_2^{2-}$ and $UO_2(CO_3)_3^{4-}$ to form U-rich hydrothermal fluids that facilitated U mineralization.

6.2 Geochronology

During Indosinian tectonism, the Yangtze and Cathaysian plates were amalgamated to form a continent in South China. Subsequently, within-plate tectonic activity has been dominant in the region [29,30]. Yanshanian tectonism was characterized by collision in the Jurassic and a change to extension in the Cretaceous. The Early Cretaceous (139–143 Ma) marked the period of this tectonic change in South China [5,6,30,31,45]. Magmatism, NNE-SSW-trending faults, and formation of extensional basins accompanied the extensional tectonism.

The Miaoershan area in western South China underwent a similar tectonic history as the South China. The CHIME (231 ± 28 Ma; 230 ± 38 Ma) and LA-ICP-MS U-Pb isotopic ages of monazite and xenotime (220 ± 6 Ma; 211 ± 7 Ma) of the present study are consistent with the single zircon SHRIMP U-Pb age of 228 ± 11 Ma for the Douzhashan granite obtained by Xie et al. [13]. These ages demonstrate that the Douzhashan granite is a late syn-collision or post-collision pluton emplaced during Indosinian tectonism. Subsequently, the Xiaomulan and Chaping granites (167 Ma [14]), the NNE-SSW-trending Xinzi Fault, the NE-SW to NNE-SSW-trending Xinzi grabens, and Cretaceous-Tertiary mafic dikes were produced in response to the tectonic extension in the Yanshanian. CHIME dating of secondary apatite in the Douzhashan granite yields an age of 136 ± 17 Ma, which coincides with the timing of Cretaceous-Tertiary extension in South China (135–140 Ma [5,30,31]).

Cretaceous-Tertiary crustal extension in South China was associated with upward migration of mantle-derived CO_2 [5,30,42,48,49]. Heat associated with the intrusion of mafic magmas drove circulation of the CO_2-rich hydrothermal fluids within fault systems. Such fluids enriched in CO_2, Ca, F, and P may have caused the breakdown of accessory minerals to synchisite or apatite and released U from primary accessory minerals. Mineral-bound U was released to fluids as soluble $UO_2(CO_3)_2^{2-}$ and $UO_2(CO_3)^{4-}$, thereby contributing to formation of the U ore deposit.

In summary, the U-rich source rocks of the Douzhashan granite formed during the Indosinian orogeny. Following this, Cretaceous-Tertiary regional crustal extension was associated with mafic dike intrusion and upward migration of mantle-derived CO_2. These hydrothermal CO_2-rich fluids scavenged U from the pre-existing U-rich granites and U was then deposited in faults and fractures to form vein-type U ore deposits. Therefore, the combination of Indosinian compressional tectono-magmatism and later Yanshanian extensional overprinting were essential in the formation of these U ore deposits.

The authors thank Wu Fuyuan, Yang Jinhui, and Liu Zhichao from the Institute of Geology and Geophysics, Chinese Academy of Sciences for technical assistance with the LA-ICP-MS analyses. This work was supported by the National Natural Science Foundation of China (41072028, 41230315 and 40702012), the National Basic Research Program of China (2012CB416704), the China Nuclear Geological Survey Basic Research Program (2011–2015), and the Doctoral Fund of the Ministry of Education of China (20100091110048).

1 Cuney M. The extreme diversity of uranium deposits. Miner Deposits, 2009, 44: 3–9
2 Du L T. Classification and genetic analysis of hydrothermal uranium deposit in China (in Chinese). Radiogeol, 1980, 3: 1–10
3 Du L T. Collected Works of Granite Type Uranium Deposit (in Chinese). Beijing: Atomic Energy Press, 1982. 1–99
4 Yu D G, Wu R G, Chen P R. Uranium Resources Geology Tutorial (in Chinese). Harbin: Harbin Institute of Technology Press, 2005. 1–20
5 Hu R Z, Bi X W, Zhou M F, et al. Uranium metallogenesis in South China and its relationship to crustal extension during the Cretaceous to Tertiary. Econ Geol, 2008, 103: 583–598
6 Chen P R. Geodynamic setting of Mesozoic magmatism and its relationgship to uranium metallogenesis in southeastern China (in Chinese). Uran Geol, 2004, 20: 266–270
7 Hua R M, Chen P R, Zhang W L, et al. Metallogeneses and their geodynamic settings related to Mesozoic granitoids in the Nanling Range (in Chinese). Geol J Chin Univ, 2005, 11: 291–304
8 Hua R M, Chen P R, Zhang W L, et al. Three major metallogenic events in Mesozoic in South China (in Chinese). Miner Deposits, 2005b, 24: 100–107
9 Chen Y W, Bi X W, Hu R Z, et al. Comparison of geochemical characteristic of uranium- and non-uranium-bearing Indosinian granites in Guidong composite pluton (in Chinese). J Miner Petrol, 2009, 29: 106–114
10 Ling H F. Origin of hydrothermal fluids of granite-type uranium deposits: Constraints from redox conditions (in Chinese). Geol Rev, 2011, 57: 193–206
11 Liu J S, Zhang B T. Tectonic alteration and uranium mineralization. Geotecton Metall, 1989, 13: 168–175
12 Fang S Y, Fan L T, Zhu K R, et al. Study on mineralization structures of vein shape granite type uranium deposit and prospecting prognosis in Menggongjie (in Chinese). Uran Geol, 2007, 23: 138–144
13 Xie X H, Chen W F, Zhao K D, et al. Geochemical characteristics and geochronology of the Douzhashan granite, northeastern Guangxi, China (in Chinese). Acta Petrol Sin, 2008, 24: 1302–1312
14 Shi S H, Hu R Z, Wen H J, et al. A tentative discussion on fluid inclusions in quartz veins of Shazijiang uranium ore deposit, northern Guangxi (in Chinese). Acta Geol Sin, 2010, 84: 1175–1182
15 Wang Z C. Mesozoic crust-deriving magmatism and uranium metallogenesis in Nanling Range of Hunan and Guangxi (in Chinese). Dissertation for the Doctoral Degree. Nanjing: Nanjing University, 2003
16 Gao S, Luo T C, Zhang B R, et al. Structure and composition of the continental crust in east China. Sci China Ser D-Earth Sci, 1999, 42:

129–140
17 No. 310 Party of Hunuan Nuclear Industry Geological Bureau. Research Report on the Relationship Between Granites and Uranium Mineralization in Central Miaoershan Region (in Chinese), 1995
18 Zhou J X, Mao S H. Electron Microprobe Analysis (in Chinese). Beijing: Geological Publishing House, 1988. 1–210
19 Suzuki K, Adachi M. Middle Precambrian detrital monazite and zircon from the Hida gneiss on Oki-Dogo Island, Japan: Their origin and implications for the correlation of basement gneiss of southwest Japan and Korea. Tectonophys, 1991, 235: 277–292
20 Suzuki K, Kato T. CHIME dating of monazite, xenotime, zircon and polycrase: Protocol, pitfalls and chemical criterion of possibly discordant age data. Gondwana Res, 2008, 14: 569–586
21 Kato T, Suzuki K, Adachi M. The computer program for the CHIME age calculation. J Earth Planet Sci Nagoya Univ, 1999, 46: 49–56
22 Kosler J, Mike N T, Paul J S. Application of llaser ablation ICP-MS to U-Th-Pb dating of monazite. Geostand Newslett, 2001, 25: 375–386
23 Paquette J L, Tiepolo M. High resolution (5 μm) U-Th-Pb isotope dating of monazite with excimer laser ablation (ELA)-ICPMS. Chem Geol, 2007, 240: 222–237
24 Liu Z C, Wu F Y, Guo C L, et al. *In situ* U-Pb dating of xenotime by laser ablation LA-ICP-MS. Chin Sci Bull, 2011, 27: 2948–2956
25 Liu Z C, Wu F Y, Yang Y H, et al. Neodymium isotopic compositions of the standard monazites used in U-Th-Pb geochronology. Chem Geol, 2012, 334: 221–239
26 Griffin W L, Powell W J, Pearson N J, et al. GLITTER: Data reduction 1164 software for laser ablation ICP-MC. Laser Ablation-ICP-MS in the Earth Sciences: 1165 Current Practices and Outstanding Issues: In: Sylvester P, ed. Mineralogical 1166 Association Canada Short Course, 2008, 40: 308–311
27 Förster H J. The chemical composition of REE-Y-Th-U-rich accessory minerals in peraluminous granites of the Erzgebirge-Fichtelgebirge region, Germany, Part I: The monazite-(Ce)-brabantite solid solution series. Am Mineral, 1998, 83: 259–272
28 Förster H J. The chemical composition of REE-Y-Th-U-rich accessory minerals from peraluminous granites of the Erzgebirge-Fichtelgebirge region, Germany. Part II: Xenotime. Am Mineral, 1998, 83: 1302–1315
29 Zhang Q W, Huang H Z. The evolution of magmatic-tectonic activation of the Meso-Cenozoic era in Eastern China. Acta Geol Sin, 1982, 2: 111–122
30 Hu R Z, Bi X W, Su W C, et al. The relationship between uranium metallogenesis and crustal extension during the Cretaceous-Tertiary in South China. Earth Sci Front, 2004, 11: 153–160
31 Li X H, Hu R Z, Rao B. Geochronology and geochemistry of Cretaceous mafic dikes from Northern Guangdong, SE China. Geochimica, 1997, 26: 14–31
32 Poitrasson F, Chenery S, Bland D J. Contrasted monazite hydrothermal alteration mechanisms and their geochemical implications. Earth Planet Sci Lett, 1996, 145: 79–96
33 Finger F, Broska I, Roberts M P, et al. Replacement of primary monazite by apatite-allanite-epidote coronas in an amphibolites facies granite gneiss from the eastern Alps. Am Mineral, 1998, 83: 248–258
34 Broska I, Williams C T, Janák M, et al. Alteration and breakdown of xenotime-(Y) and monazite-(Ce) in granitic rocks of the Western Carpathians, Slovakia. Lithos, 2005, 82: 71–83
35 Broska I, Williams C T, Petrík I. Coexisting monazite and allanite in peraluminous granitoids of the Tribeč Mountains, Western Carpathians. Am Mineral, 2000, 85: 22–32
36 Dini A, Rocchi S, Westerman D S. Reaction microtextures of REE-Y-Th-U accessory minerals in the Monte Capanne pluton (Elba Island, Italy): A possible indicator of hybridization processes. Lithos, 2004, 78: 101–118
37 Hecht L, Cuney M. Hydrothermal alteration of monazite in the Precambrian crystalline basement of the Athabasca Basin (Saskatchewan, Canada): Implications for the formation of unconformity-related uranium deposits. Miner Deposits, 2000, 35: 791–795
38 Mathieu R, Zetterström L, Cuney M, et al. Alteration of monazite and zircon and lead migration as geochemical tracers of fluid paleocirculations around the Oklo-Oke´lobondo and Bangombe´natural nuclear reaction zones (Franceville basin, Gabon). Chem Geol, 2001, 171: 147–171
39 Eggleton R, Banfield J. The alteration of granitic biotite to chlorite. Am Mineral, 1985, 70: 902–910
40 Lanzirotti A, Hanson G. Geochronology and geochemistry of multiple generations of monazite from the Wepawaug Schist, Connecticut, USA: implications for monazite stability in metamorphic rocks. Contri Mineral Petrol, 1996, 125: 332–340
41 Chao R, Xia L. Genesis and Implication of Fluid and Melt Inclusions within Mantle Xenoliths Discovered in Xilong, Zhejiang Province: Compiled Papers on China's Upper Mantle Characteristics and Dynamics (in Chinese). Beijing: Seismological Publishing House, 1990. 14–22
42 Hu R Z, Jin J F. Mechanism of the migration and deposition of uranium in ascending hydrothermal solutions: Evidence from the Xiwang uranium deposit (in Chinese). Geol Rev, 1990, 36: 325–331
43 Zhao H, Deng J. The Characteristics of Plutonism in the Upper Mantle along the Coastal Areas of Southeast China, in China's Upper Mantle Characteristics and Dynamics (in Chinese). Beijing: Seismological Publishing House, 1990. 62–71
44 Leory J. The Margnac and Fanay uranium deposits of the La Crouzille district (western Massif Central, France): Geologic and fluid inclusion studies. Econ Geol, 1978, 73: 1611–1634
45 Hu R Z, Li C Y, Ni S J, et al. Research on $\sum CO_2$ source in ore-forming hydrothermal solution of granite-type uranium deposit, South China. Sci China Ser D-Earth Sci, 1993, 36: 1252–1262
46 Zhang Z S, Hua R M , Wu J H, et al. Mineralization mechanism and geodynamic setting of No.337 deposit in Xiazhuang uranium orefield (in Chinese). Uran Geol, 2009, 25: 1–6
47 Veblen D, Ferry J. A TEM study of the biotite-chlorite reaction and comparison with petrologic observation. Am Mineral, 1983, 68: 1160–1168
48 Chen Y H, CHen Z Y, Cai Y Q, et al. Space time evolution of Meso-Cenozoic extensional tectonics and distributions of uranium mineralization in southeastern China (in Chinese). Uran Geol, 1997, 13: 129–146
49 Qi H W, Hu R Z. Comparison between uranium ore-forming fluids and magmatic fluids of granites, South China (in Chinese). Acta Mineral Sin, 2000, 20: 401–405